Optical preparation and detection of spin coherence in molecules and crystal defects

Lof, Gerrit

DOI:
10.33612/diss.109567350

Chapter 4

Proposal for time-resolved optical probing of electronic spin coherence in divacancy defects in SiC

Abstract

The Time-Resolved Faraday Rotation (TRFR) technique is an all-optical non-invasive measurement technique which can provide a measure of electron spin dynamics and is usually applied to materials with strong spin-orbit coupling. We propose for the first time to use this technique to characterize spin active color centers in materials with negligible spin-orbit coupling, like silicon carbide and diamond. The fundamentals and scenario for a TRFR experiment are here worked out for a homogeneous ensemble of c-axis divacancies in silicon carbide. We demonstrate that one of the indices of refraction of this material oscillates as a function of time in the presence of coherences. Due to this time-dependent birefringence, a probe pulse will undergo a polarization rotation as a function of the pump-probe delay time. This polarization rotation is a measure for the spin coherence of the triplet excited state.

This chapter is based on Ref. 3 on p. 177.

4.1 Introduction

The implementation of solid-state based quantum networks relies fundamentally on the possibility of initializing, manipulating and reading the information contained in a qubit[83]. Optical implementation of these operations increases the processing rates and simplify the network architecture, enabling faster and simpler circuits[84]. In this scenario, probing of the electronic spin (dynamics) based on the polarization rotation (referred to as Faraday and Kerr rotation for the case of transmission and reflection, respectively) of laser light has been extensively applied to the investigation of localized electronic states embedded in III-V and II-VI semiconductors[13, 46]. As compared to other optical techniques such as optically detected magnetic resonance and resonant absorption, these techniques have the advantage that they can preserve the coherence of the measured state[85], allowing further operations to be performed. Furthermore, since the polarization rotation measurements rely on the dispersive scattering of a large number of photons, they are less susceptible to photon losses and can usually be implemented without optical microcavities[59]. Finally, these techniques can be performed in a time-resolved manner, enabling the investigation of the time-evolution of the electronic spin with outstanding resolution.

In III-V and II-VI semiconductors, strong spin-orbit coupling (SOC) generates spin-dependent optical selection rules[9], such that the spin-state of a system is directly mapped into a shift of the polarization of a laser beam interacting with the material. In contrast, silicon carbide (SiC) and diamond, some of the most promising materials for the implementation of solid-state qubits, show negligible SOC. Nonetheless, in this theoretical work we demonstrate for SiC c-axis divacancies (missing neighboring Si and C atom along the growth axis) that the polarization of a probe pulse can also provide information about the spin-coherence in these systems due to effective selection rules that emerge from the symmetry of these localized triplet electronic states. Due to the axial symmetry of the system, the degeneracy within the ground and excited states is broken, generating a characteristic zero-field splitting (ZFS) in the absence of a magnetic field[86, 87]. If the ZFS of the ground and excited states is different, a weak magnetic field enables spin-flipping transitions with probabilities determined by the Franck-Condon factors for spin. This generates a dependency between the specific configuration of the electronic spin and the total transition probability between the ground and excited states. Accordingly, the linear susceptibility tensor (which governs the optical refractive indices) is modulated by the coherent

spin precession of the system. In this way, time-resolved measurement of the polarization rotation allows for characterization of the electronic spin (dynamics) for systems with negligible SOC like many types of color centers in SiC and diamond, to which this technique has never been applied.

4.2 Fundamentals for a TRFR experiment with a homogeneous ensemble of c-axis divacancies in SiC

For a proof of principle calculation of a Time-Resolved Faraday Rotation (TRFR) experiment (Fig. 4.1) applied to color centers in SiC, we consider an ultrashort polarized pump pulse that excites a homogeneous ensemble of c-axis divacancies in SiC from their triplet ground state (after preparation in the required state)

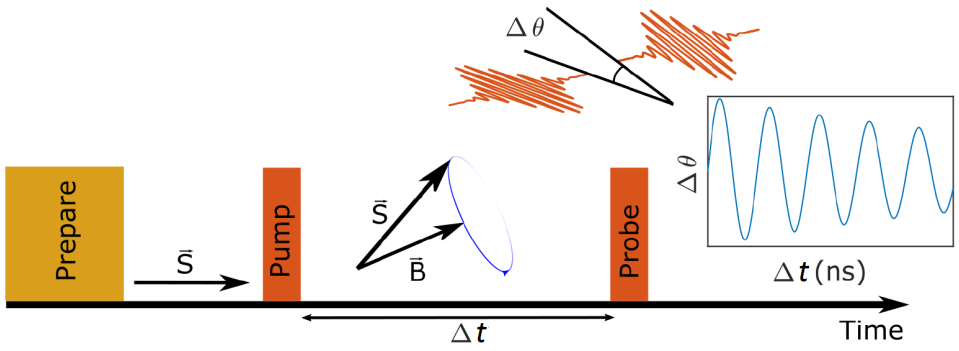

Figure 4.1: Outline of a TRFR experiment. After the sample is prepared in a certain quantum state, it gets excited by a pump pulse to a superposition of excited state sublevels. Before a probe pulse arrives, the system remains in the dark during the pump-probe delay time Δt. The change of the polarization of the probe depends on the degree of birefringence of the sample at the time it gets hit by the probe. Measuring this change (usually the polarization rotation $\Delta\theta$) as a function of Δt gives a time-resolved image of the spin dynamics of the system. For a superposition of two excited state sublevels, the TRFR signal has a single frequency. A beating of up to three frequencies (corresponding to the energy differences) can occur for a superposition of three sublevels. Decoherence is expressed by a decay of the TRFR signal as a function of time. Analogously, for a probing of ground state coherence, one should prepare the system first in the excited state in order to create and probe a superposition of ground state sublevels.

into a superposition of sublevels of their lowest triplet excited state (Fig. 4.2a). Such a superposition ($|\psi_e(t)\rangle$ in Fig. 4.2b) will show spin precession as a function of time. We will derive that in addition also one of the indices of refraction of the material oscillates with time. Hence, the polarization of an ultrashort probe pulse is affected (upon transmission), since its components experience a different real part of the refractive index[16], as is worked out in more detail in Chapter 3. Specifically, the polarization rotation $\Delta\theta$ as a function of the (pump-probe) delay time Δt (Fig. 4.1, 4.2b) is a measure for the spin dynamics in the system. For a superposition of two excited state sublevels, the TRFR signal has a single frequency. A beating of up to three frequencies (corresponding to the energy differences of the spin sublevels in the excited state) can occur for a superposition of three sublevels. Taking a detuned probe limits population transfer back to the ground state sublevels, which allows to consider dispersion only[54]. In this section (4.2) we derive for a homogeneous ensemble of SiC divacancies the fundamentals of a TRFR experiment. Although this derivation is quite general, we make in Fig. 4.2 and Section 4.3 several assumptions (like excited state coherence for two sublevels only) for the sake of simplicity.

If we assume that in SiC c-axis divacancy defects the SOC effects have negligible influence, the Hamiltonian describing the ground(excited) state is given by[86, 88, 89]

$$\begin{aligned} H_{g(e)} &= hD_{g(e)}S_z^2 + g_{g(e)}\mu_B\vec{B}\cdot\vec{S} \\ &= hD_{g(e)}S_z^2 + g_{g(e)}\mu_B(S_xB_x + S_yB_y + S_zB_z) \end{aligned} \tag{4.1}$$

where the zero-field splitting $D_{g(e)}$ is determined by the spatial distribution of the ground(excited) state. S_i is the spin S=1 operator in the i direction, $\vec{B}$ is the magnetic field, $g_{g(e)}$ is the g-factor for the ground(excited) state and μ_B is the Bohr magneton.

Due to the absence of SOC, the eigenstates of the Hamiltonian can be written as a product of a spatial part $|\chi\rangle$ and a spin state. In this way, the eigenstates of the ground (excited) state Hamiltonian are (in the basis of the total Hamiltonian in Eq. 4.1) given by $\left|\chi_{g(e)}\right\rangle|g(e)_i\rangle$, where $i = l, m, u$ correspond to the spin of lowest, median and upper energy, respectively (as illustrated in Fig. 4.2, where the orbital part is neglected). The Frank-Condon factor for spin, which determines the overlap between a sublevel i of the ground-state Hamiltonian and a sublevel j of the excited-state Hamiltonian, is given by $\langle e_j|g_i\rangle$. If the zero-field splittings for the ground and excited state are different, i.e. if $D_g \neq D_e$, all nine

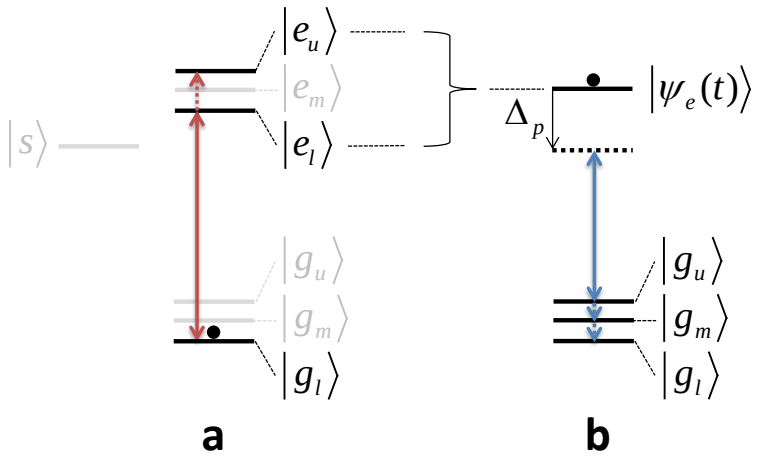

Figure 4.2: Schematic of the (de)tuning of the pump and probe pulse for a TRFR experiment with a homogeneous ensemble of c-axis divacancies in SiC. Although Section 4.2 describes the fundamentals for quite general conditions, several assumptions are made in this figure for the sake of simplicity. **a**, We assume that the system is prepared with its population only in the lowest ground state sublevel. With $\vec{B} \perp$ to the c-axis, several transitions remain forbidden, such that we can neglect $|e_m\rangle$ in this example. Just before the pump pulse (red arrow) arrives at $t = 0$, only $|g_l\rangle$ is populated, as indicated with the dot. Full absorption of a photon out of a short optical pump pulse induces the state $|\psi_e(t = 0)\rangle$, being a superposition of $|e_l\rangle$ and $|e_u\rangle$ (we neglect here the orbital part, Eq. 4.2). **b**, Directly after excitation with the pump, $|\psi_e(t)\rangle$ is populated as indicated with the dot. A linear probe pulse (blue arrow) with detuning Δ_p experiences a polarization rotation $\Delta\theta$, which oscillates as a function of the delay time Δt. This oscillation is a measure for the spin precession related to the coherence of $|\psi_e(t)\rangle$.

transitions (from the three sublevels of the ground state to the three sublevels of the excited state) are allowed, unless $\vec{B} \perp$ to the c-axis. In that special case, some transitions remain still forbidden, as derived in Supplementary Information Section 4.7 (p. 112).

Alternative non-radiative decay paths from levels $|e_j\rangle$ to $|g_i\rangle$ are possible via the intermediate singlet state $|s\rangle$[90]. This process, known as intersystem crossing (ISC) (which also occurs for nitrogen-vacancy (NV^-) centers in diamond[91]), allows for high-fidelity preparation of the initial quantum state (via a continuous wave laser which should be turned off just before the pump pulse arrives, Fig. 4.1) via preferred relaxation into $|g_l\rangle$.

For simplicity, we assume in Fig. 4.2 and Section 4.3 that (before the pump-pulse arrives) the divacancies are prepared with all the population in the lowest

sublevel of the ground-state, i.e. $|\psi_{prep}\rangle = |\chi_g\rangle\,|g_l\rangle$. Also, we assume that $\vec{B} \perp$ to the c-axis, such that certain optical transitions remain forbidden. However, we will consider the general case for the following derivation of the polarization change of a probe pulse within a TRFR experiment applied to SiC with a homogeneous ensemble of c-axis divacancies.

At time $t = 0$, the system is excited by the pump-pulse which brings the divacancies into a state described by

$$|\psi_e(t=0)\rangle = |\chi_e\rangle\,(c_l\,|e_l\rangle + c_m\,|e_m\rangle + c_u\,|e_u\rangle) \tag{4.2}$$

where the normalization coefficients c_i are proportional to $\langle e_i|g_l\rangle$.

Thus, for a SiC divacancy in an excited state given by $|\psi_e(t)\rangle = \sum_i c_i(t)\,|\psi_{e,i}\rangle$, the driven coherent transition rate into the j-th eigenvector of the ground state Hamiltonian $|\psi_{g,j}\rangle$, via excitation with an optical field, is given by the Rabi frequency

$$\Omega_j = \frac{\vec{E}\cdot\vec{\mu}_{e\to j}}{\hbar} = \frac{\langle\psi_e(t)|\,\vec{E}\vec{r}\,|\psi_{g,j}\rangle}{\hbar} \tag{4.3}$$

The total transition rate into the ground state is given by

$$\begin{aligned}\Omega = \sum_j \Omega_j &= \sum_j \frac{\langle\psi_e|\,\vec{E}\vec{r}\,|\psi_{g,j}\rangle}{\hbar} = \sum_{i,j} -e\frac{\langle\chi_e|\,(E_x x + E_y y + E_z z)\,|\chi_g\rangle}{\hbar} c_i(t)\,\langle e_i|g_j\rangle \\ &= \sum_{\alpha=x,y,z} E_\alpha \frac{-e}{\hbar}\,\langle\chi_e|\,\alpha\,|\chi_g\rangle \sum_{i,j} c_i(t)\,\langle e_i|g_j\rangle = \sum_\alpha \frac{E_\alpha d^\alpha}{\hbar} \sum_{i,j} c_i(t)\,\langle e_i|g_j\rangle\end{aligned} \tag{4.4}$$

where we have defined $d^\alpha \equiv -e\,\langle\chi_e|\,\alpha\,|\chi_g\rangle$. By combining Eq. 4.3 and 4.4, we can thus write for $\mu^\alpha_{e(\to)g}$

$$\mu^\alpha_{eg} = d^\alpha \sum_{i,j} c_i(t)\,\langle e_i|g_j\rangle \tag{4.5}$$

The linear susceptibility tensor of the medium, which describes how the medium interacts with light polarized in the x, y, z directions, has components

$$\tilde{\chi}^{(1)}_{\alpha\beta} = \frac{N}{\epsilon_0\hbar}\Big(\frac{\Delta_p - i\gamma}{\Delta_p^2 + \gamma^2}\Big)\mu^\alpha_{eg}\mu^\beta_{ge} \tag{4.6}$$

where the tilde denotes a complex number, N is the number density of defects, ϵ_0 is the vacuum permittivity, $\hbar$ is the reduced Planck's constant, Δ_p is the detuning between the driving field and the transition frequency of the system, and γ is the damping rate of the system. Substituting the transition dipole moments obtained from Eq. 4.5 into Eq. 4.6, we get

$$\tilde{\chi}^{(1)}_{\alpha\beta} = \frac{N}{\epsilon_0 \hbar}\Big(\frac{\Delta_p - i\gamma}{\Delta_p^2 + \gamma^2}\Big) d^{\alpha} d^{\beta *} \phi(t) \tag{4.7}$$

with the time-dependent term $\phi(t)$ defined as

$$\phi(t) = \sum_{w,v} c_w(t) \langle e_w | g_v \rangle \sum_{i,j} c_i^*(t) \langle g_j | e_i \rangle = \sum_{w} c_w(t) \langle e_w | \sum_{v,j} |g_v\rangle \langle g_j| \sum_{i} c_i^*(t) |e_i\rangle \tag{4.8}$$

We define the operator $\mathbf{O} = \sum_{v,j} |g_v\rangle \langle g_j|$, which is clearly Hermitian. In these terms, the expression for $\phi(t)$ obtained in Eq. 4.8 can be simplified as

$$\begin{aligned} \phi(t) &= \sum_{w,i} c_w(t) c_i^*(t) \langle e_w | \mathbf{O} | e_i \rangle \\ &= \sum_{i} |c_i(t)|^2 \langle e_i | \mathbf{O} | e_i \rangle + \sum_{w<i} [c_w(t) c_i^*(t) \langle e_w | \mathbf{O} | e_i \rangle + c_w^*(t) c_i(t) \langle e_i | \mathbf{O} | e_w \rangle] \end{aligned} \tag{4.9}$$

Since the operator $\mathbf{O}$ is Hermitian, the term $\langle e_i | \mathbf{O} | e_i \rangle$ is real and $\langle e_w | \mathbf{O} | e_i \rangle = \langle e_i | \mathbf{O} | e_w \rangle^*$, which yields

$$\phi(t) = \sum_{i} |c_i(t)|^2 O_{ii} + \sum_{w<i} [O_{wi} c_w(t) c_i^*(t) + c.c.] \tag{4.10}$$

where we have defined $O_{ij} \equiv \langle e_i | \mathbf{O} | e_j \rangle$, and the abbreviation *c.c.* denotes the complex conjugate of $O_{wi} c_w(t) c_i^*(t)$. Thus, $\phi(t)$ is real valued, and (the second term) varies in time. Since the operator $\mathbf{O}$ is time-independent, the time-dependence of $\phi(t)$ comes directly from the time-evolution of the excited state given by $c_i(t)$.

Previous work revealed that the absorption of c-axis divacancies in SiC happens only for light polarized along the basal plane[87]. This means that if $\hat{z}$ coincides with the c-axis, $d^z = 0$, and the first-order susceptibility tensor is given by

$$\tilde{\chi}^{(1)} = \frac{N}{\epsilon_0 \hbar}\Big(\frac{\Delta_p - i\gamma}{\Delta_p^2 + \gamma^2}\Big)\phi(t) \begin{bmatrix} d^{x*}d^x & d^{x*}d^y & 0 \\ d^{y*}d^x & d^{y*}d^y & 0 \\ 0 & 0 & 0 \end{bmatrix} \tag{4.11}$$

This matrix can be diagonalized, so that in its eigenbasis $\{\hat{x}', \hat{y}', \hat{z}'\}$ it is given by

$$\tilde{\chi}^{(1)} = \frac{N}{\epsilon_0 \hbar}\Big(\frac{\Delta_p - i\gamma}{\Delta_p^2 + \gamma^2}\Big)\phi(t) \begin{bmatrix} d_0^2 & 0 & 0 \\ 0 & 0 & 0 \\ 0 & 0 & 0 \end{bmatrix} \tag{4.12}$$

where we have defined $d_0^2 = d^{x*}d^x + d^{y*}d^y$. Its eigenvectors are given by

$$\begin{aligned} \hat{x}' &= \frac{d^{x*}\hat{x} + d^{y*}\hat{y}}{d_0} \\ \hat{y}' &= \frac{-d^y\hat{x} + d^x\hat{y}}{d_0} \\ \hat{z}' &= \hat{z} \end{aligned} \tag{4.13}$$

Here we can note the difference between the case considered in this chapter compared to Chapter 3. There, the polarization selection rules for the transition to different eigenvectors of the excited state give a time-dependence specific to each component of the susceptibility tensor, implying that the eigenbasis of the susceptibility tensor is time-dependent. In contrast, in the current chapter the eigenbasis is time-independent, whereas the time-dependence for the components of $\tilde{\chi}^{(1)}$ originates from $\phi(t)$.

Once the susceptibility tensor is diagonalized, we can calculate the complex refractive indices $\tilde{n}_\alpha = \sqrt{1 + \tilde{\chi}^{(1)}_{\alpha\alpha}} \approx 1 + \tilde{\chi}^{(1)}_{\alpha\alpha}/2$ of the material in the direction of the eigenvectors of $\tilde{\chi}^{(1)}$, i.e.

$$\begin{aligned} \tilde{n}_{x'} &= 1 + \frac{N d_0^2}{2\epsilon_0 \hbar}\Big(\frac{\Delta_p - i\gamma}{\Delta_p^2 + \gamma^2}\Big)\phi(t) \\ \tilde{n}_{y'} &= 1 \\ \tilde{n}_{z'} &= 1 \end{aligned} \tag{4.14}$$

Thus, the sample functions as a birefringent plate, such that the electric field components of the probe pulse along the $\hat{z}'$ and $\hat{y}'$ directions propagate as they would in the bulk material (unaffected by divacancy transitions), while the component along the $\hat{x}'$ direction feels the presence of the divacancy defects in a time-dependent way.

The Jones matrix formalism allows us to calculate the polarization and ellipticity of an outcoming beam after it interacts with a sample whose principal axes have different refractive indices, $n_{x'}$ and $n_{y'}$. In the basis of the principal axes of the sample $\{\hat{x}', \hat{y}'\}$, the Jones matrix describing the effect of the interaction with the sample on the propagating electromagnetic field is given by

$$J_{\hat{x}',\hat{y}'} = \begin{bmatrix} e^{i\Lambda n_{x'}} & 0 \\ 0 & e^{i\Lambda n_{y'}} \end{bmatrix} \tag{4.15}$$

where $\Lambda = 2\pi d/\lambda$, with d denoting the thickness of the sample, and λ the wavelength of light. A multiplication by a common phase factor yields

$$J_{\hat{x}',\hat{y}'} = \begin{bmatrix} e^{i\Lambda\Delta n} & 0 \\ 0 & 1 \end{bmatrix} \tag{4.16}$$

where $\Delta n = n_{x'} - n_{y'}$. The matrix $T_{\hat{x},\hat{y}\to\hat{x}',\hat{y}'}$

$$T_{\hat{x},\hat{y}\to\hat{x}',\hat{y}'} = \frac{1}{d_0}\begin{bmatrix} d^{x*} & d^{y*} \\ -d^{y} & d^{x} \end{bmatrix} \tag{4.17}$$

allows us to write the Jones matrix in the $\{\hat{x}, \hat{y}\}$ basis, such that

$$\begin{aligned} J_{\hat{x},\hat{y}} =& T^{-1}_{\hat{x},\hat{y}\to\hat{x}',\hat{y}'} J_{\hat{x}',\hat{y}'} T_{\hat{x},\hat{y}\to\hat{x}',\hat{y}'} \\ J_{\hat{x},\hat{y}} =& \frac{1}{d_0^2}\begin{bmatrix} d^{x} & -d^{y*} \\ d^{y} & d^{x*} \end{bmatrix}\begin{bmatrix} e^{i\Lambda\Delta n} & 0 \\ 0 & 1 \end{bmatrix}\begin{bmatrix} d^{x*} & d^{y*} \\ -d^{y} & d^{x} \end{bmatrix} \\ J_{\hat{x},\hat{y}} =& \frac{1}{d_0^2}\begin{bmatrix} |d^x|^2 e^{i\Lambda\Delta n} + |d^y|^2 & d^x d^{y*}(e^{i\Lambda\Delta n} - 1) \\ d^{x*} d^y (e^{i\Lambda\Delta n} - 1) & |d^y|^2 e^{i\Lambda\Delta n} + |d^x|^2 \end{bmatrix} \end{aligned} \tag{4.18}$$

After interacting with the sample, the electromagnetic field is transformed such that

$$\vec{E}_{out} = J_{\hat{x},\hat{y}}\vec{E}_{in} \tag{4.19}$$

where $\vec{E}_{in}$ and $\vec{E}_{out}$ are the incoming and outcoming beam, respectively. Within the Jones formalism, the generalized electric field vector $\vec{E}_{in}$ of an incoming beam (normalized and global phase factor set to zero) in terms of the azimuth θ and the ellipticity ϵ is given by Eq. 1.2, i.e.

$$\vec{E}_{in} = E_0 \begin{bmatrix} \cos(\theta)\cos(\epsilon) - i\sin(\theta)\sin(\epsilon) \\ \sin(\theta)\cos(\epsilon) + i\cos(\theta)\sin(\epsilon) \end{bmatrix} \tag{4.20}$$

It is convenient (following the Cartesian complex-plane representation of polarized light as in [16] and analogous to Chapter 3) to define the ratio

$$\kappa = E_x/E_y \tag{4.21}$$

After substituting Eq. 4.20 and 4.18 into 4.19, one can calculate the change in the azimuth $\Delta\theta = \theta_{out} - \theta_{in}$ and the change in the ellipticity $\Delta\epsilon = \epsilon_{out} - \epsilon_{in}$ from

$$\tan 2\theta = \frac{\kappa^* + \kappa}{1 - |\kappa|^2} \tag{4.22}$$

and

$$\sin 2\epsilon = \frac{i(\kappa^* - \kappa)}{1 + |\kappa|^2} \tag{4.23}$$

respectively.

4.3 Estimating the polarization rotation of a linear probe for a TRFR experiment with c-axis divacancies in SiC

4.3.1 Assumptions and parameters

To determine whether a TRFR experiment can be applied to SiC divacancies, we will in this section calculate $\Delta\theta(\Delta t)$, i.e the polarization rotation as a function of the pump-probe delay time, based on the parameters (Table 4.1) and assumptions that we here elaborate on.

We will here consider a TRFR experiment applied to a homogeneous ensemble of c-axis divacancies (C_{3v} symmetry) in a SiC sample with thickness $d = 2$

mm and a divacancy number density of $N = 10^{16}$ cm^{-3}, based on [87]. For an inhomogeneously broadened ensemble, the TRFR signal will drop, typically proportional to $1/\sigma$, with σ the standard deviation of the inhomogeneous broadening[92]. For the initially prepared state (before the pump pulse arrives), we assume that only the lowest ground state sublevel is populated, i.e. $|\psi_{prep}\rangle = |g_l\rangle$. It is assumed that the transition dipole moments are equal for the x and y direction, i.e. $|d^x| = |d^y| = d_0/\sqrt{2}$, based on previous work showing a weak polarization dependence on the transition dipoles in the basal plane[86, 87]. We have estimated $d_0 = 6.4 \cdot 10^{-32}$ C·m, as worked out in Supplementary Information Section 4.6 (p. 111). For both the pump and probe we assume a transition wavelength of 1082 nm (corresponding to $E_e - E_g$, with $E_{g(e)}$ the ground(excited) state energy), although the probe will be slightly detuned. We take the incoming pump and probe pulse polarized along the x-direction (i.e. both having $\theta_{in} = 0$). We assume that the delay time Δt between pump and probe is taken such that $\Delta t << \omega_{ij}^{-1}$ and $\Delta t >> \omega_{eg}^{-1}$ (with $\hbar\omega_{ij} = E_{e,i} - E_{e,j}$ and $\hbar\omega_{eg} = E_e - E_g$). This ensures that the TRFR experiment will take only account of coherences between excited state sublevels (not between ground and excited state). The magnetic field is taken $B = 50$ mT, along the x-axis (perpendicular to the c-axis). This implies an excited state energy splitting $E_{e,u} - E_{e,l} \approx 1.9$ μeV (2.9 GHz angular frequency). To simultaneously address $|e_l\rangle$ and $|e_u\rangle$, we propose to use ultrashort laser pulses with an uncertainty in the photon energy given by $\sigma_{E_{ph}} > E_{e,u} - E_{e,l}$. This requires that the standard deviation of the time duration σ_t of the pulses should not exceed 0.17 ns, as follows from the time−energy uncertainty relation. It should be noted here that although any σ_t smaller than 0.17 ns satisfies the criterion of simultaneously addressing the excited state sublevels in order to cre-

Table 4.1: Parameters for a SiC divacancy TRFR experiment applied to a homogeneous ensemble of spin S=1 divacancies in SiC.

Parameter	Value
B_x ($\perp$ to c-axis)	50 mT
d	2 mm
N	10^{16} cm^{-3}
λ	1082 nm
Δ_p	-3($E_{e,u} - E_{e,l}$) = 8.7 GHz
γ	0.1 GHz
d_0	$6.4 \cdot 10^{-32}$ C·m

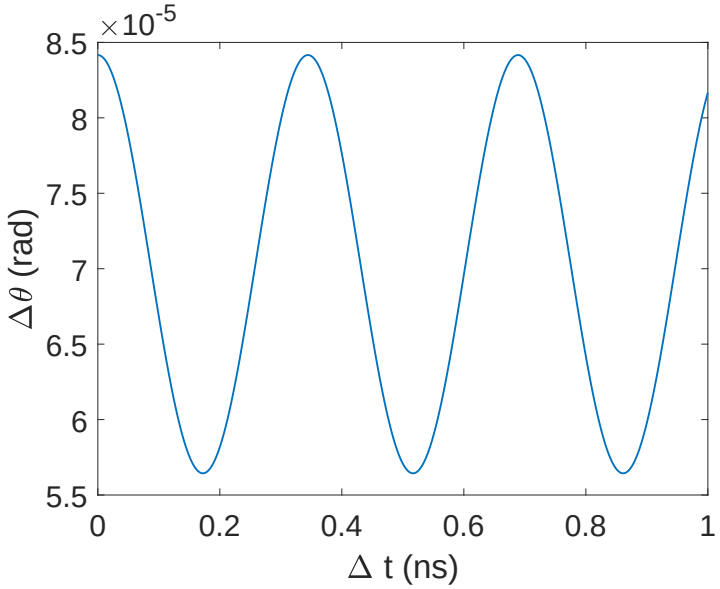

Figure 4.3: Polarization rotation $\Delta\theta$ of a probe pulse after transmission through a 2 mm SiC sample, containing a homogeneous ensemble (number density $N = 10^{16}$ cm^{-3}) of divacancies (with estimated transition dipole moment $d_0 = 6.4 \cdot 10^{-32}$ C·m. Furthermore, we consider a magnetic field along the x-axis with $B = 50$ mT, a detuning $\Delta_p = 8.7$ GHz for the probe laser, and a dephasing $\gamma = 0.1$ GHz. The incoming pump and probe pulse are linearly polarized with $\theta_{in} = 0$.

ate a superposition with the pump pulse, one should keep σ_t as close to 0.17 ns as possible in order to suppress population transfer to the ground state via the detuned probe pulse (which requires $|\Delta_p| >> |E_{e,u} - E_{e,l}|/\hbar$, which we assume to be satisfied by taking $\Delta_p = -3|E_{e,u} - E_{e,l}|/\hbar \approx -8.7$ GHz). Since most pulsed lasers have $\sigma_t << 0.17$ ns, it might (for the suppression of population transfer to the ground state) be required to use a larger magnetic field in order to increase (according to the Zeeman effect) the energy splitting $E_{e,u} - E_{e,l}$ or to take the detuning Δ_p (much) more than 3 times the sublevel splitting. We take $\gamma = 0.1$ GHz (in order to have $\Delta_p >> \gamma$). This value might be exceeded for high temperatures, but γ is in the order of MHz below 10 K[87].

4.3.2 Results and discussion

Fig. 4.3 shows the polarization rotation $\Delta\theta(\Delta t)$ (Eq. 4.22) of a linearly polarized probe pulse after transmission through a SiC sample with a homogeneous ensemble of c-axis divacancies, based on the assumptions given in Section 4.3.1.

In practice, the TRFR signal (and other oscillations) will decay as a function of (delay) time due to decoherence, which we have not taken into account in our model. Hence, the TRFR signal is to a good approximation given by the sine function $\Delta\theta = A_{\Delta\theta}\sin(\omega_{ul}\Delta t + \varphi) + b_{\Delta\theta}$, with amplitude $A_{\Delta\theta} \approx 1.4 \cdot 10^{-5}$ rad, angular frequency $\omega_{ul} = (E_{e,u} - E_{e,l})/\hbar \approx 2.9$ GHz, constant $b_{\Delta\theta} \approx 6.9 \cdot 10^{-5}$ rad, and phase $\varphi = \pi/2$ (which originate from the first and second term in Eq. 4.10, respectively).

Analogously, $\phi(t)$ (Eq. 4.10), $\Delta n(t)$ (Eq. 4.16) and the change of ellipticity $\Delta\epsilon(\Delta t)$ (Eq. 4.23) are to a good approximation sines with the same angular frequency ω_{ul} and phase φ, but different amplitudes ($A_\phi \approx 0.16$, $A_{\Delta\epsilon} \approx 1.2 \cdot 10^{-3}$ rad, $A_{\Delta n} \approx 0.2 \cdot 10^{-6}$) and constant b ($b_\phi \approx 0.84$, $b_{\Delta\epsilon} \approx 6.0 \cdot 10^{-3}$ rad, $b_{\Delta n} \approx 1.05 \cdot 10^{-6}$).

We have verified that the polarization rotation scales to a good approximation linearly with the thickness d (compare Chapter 3.9), as long as the product $\Lambda\Delta_n$ (Eq. 4.16) is small.

When the magnetic field is not taken perpendicular to the c-axis, all nine optical transitions between ground and excited state become allowed. As such, the pump pulse can induce a superposition of three excited state sublevels, which ends up as a beating of up to three frequencies in the polarization rotation $\Delta\theta(\Delta t)$ of the probe pulse (as well as in $\phi(t)$, $\Delta n(t)$ and $\Delta\epsilon(\Delta t)$).

4.4 Summary and Outlook

In SiC and diamond, SOC is weak. Nonetheless, the crystal symmetry is responsible for effective selection rules which yield a correlation between the spin-polarization of color centers and the refractive indices along the principal axes, allowing the TRFR experiment to be applied to these materials. We have worked out the fundamentals and scenario for a homogeneous ensemble of c-axis divacancies in SiC. A derivation is given for the polarization rotation of a probe pulse, induced by time-dependent birefringence. Realistic parameters and assumptions are considered, giving a polarization rotation (of the probe pulse upon transmission) of $1.4 \cdot 10^{-5}$ rad amplitude, which is well within the measurable range ($>$ nrad). If a SiC sample with an inhomogeneous ensemble of c-axis divacancies is used instead, this TRFR signal will drop, but even then it should be possible to realize a TRFR experiment[92].

4.5 Author contributions

This chapter is based on Ref. 3 on p. 177. The project was initiated by C.H.W. and C.G. Derivations, calculations and data analysis were performed by C.G., G.J.J.L and F.H. C.G and G.J.J.L. had the lead on writing the manuscript. All authors read and commented on the manuscript.

Supplementary Information (SI)

4.6 SI: Estimating the transition dipole moment of divacancies in SiC

For a monochromatic propagating wave, such as a plane wave or a Gaussian beam, the optical intensity I relates to the amplitude $|E|$ of the electric field as

$$I = \frac{c\epsilon_0 n}{2}|E|^2 \tag{4.24}$$

with c the speed of light in vacuum, ϵ_0 the vacuum permittivity, and n the refractive index.

Let us assume that our laser beam can be approximated as a Gaussian beam for which the peak intensity is given in terms of the optical power P and beam radius w as

$$I = \frac{2P}{\pi w^2} \tag{4.25}$$

Assuming that the electric field component of light is parallel to the transition dipole moment of the system of interest, the Rabi frequency (Eq. 4.3) is given by

$$\Omega = \frac{|\mu_{ij}||E|}{\hbar} \tag{4.26}$$

where μ_{ij} is the transition dipole moment related to states ψ_i and ψ_j.

From Eq. 4.24-4.26 we obtain

$$|\mu_{ij}| = \frac{\hbar}{2}\sqrt{\pi c\epsilon_0 n}\frac{\Omega w}{\sqrt{P}} \tag{4.27}$$

For a transition between the ground and (lowest) excited state of a spin S=1 SiC divacancy system, our estimate for the transition dipole moment (d_0 in the main text) is $6.4 \cdot 10^{-32}$ C·m, based on the following parameters: $n = 2.64$ corresponding to 6H-SiC at room temperature (becoming somewhat lower at cryogenic temperatures[93]), $\Omega = 7.4$ MHz, $w = 35$ μm and $P = 1$ mW, with the last three parameters based on [87].

4.7 SI: Dependency on the magnetic field angle for the optical selection rules of c-axis divacancies in SiC

The c-axis divacancy in SiC is characterized by a ground and excited state with spin 1, with addressable optical transitions and weak spin-orbit coupling. Due to this last feature, we can regard the ground(excited) state eigenvectors as a product of a spatial component (denoted by $\left|\chi_{g(e)}\right\rangle$) and a spin component ($|g(e)_i\rangle$, where $g(e)$ refers to the ground(excited) state and $i = l, m, u$ refers to the lowest, middle and upper spin eigenstates, respectively). Here, we are interested in obtaining the transition probability between ground state sublevel ($|\phi_{g,j}\rangle = |\chi_g\rangle\,|g_j\rangle$) and an excited state sublevel ($|\phi_{e,i}\rangle = |\chi_e\rangle\,|e_i\rangle$), given by $\langle\phi_{g,j}|\,\vec{\mu}\,|\phi_{e,i}\rangle$, where $\vec{\mu}$ is the electric dipole operator. Since the electric dipole operator operates on the spatial component of the electronic wavefunction, we can rewrite

$$\langle\phi_{g,j}|\,\vec{\mu}\,|\phi_{e,i}\rangle = \langle\chi_g|\,\vec{\mu}\,|\chi_e\rangle\,\langle g_j|e_i\rangle \tag{4.28}$$

which shows that the transition probability between a ground and excited state sublevel is proportional to the overlap of the spin wavefunctions, $\langle e_i|g_j\rangle$. In order to calculate this overlap as a function of magnetic field, we refer to the spin Hamiltonian describing the ground(excited) state of the c-axis divacancy defect in SiC under the action of a magnetic field, i.e.

$$H_{g(e)} = hD_{g(e)}S_z^2 + g_{g(e)}\mu_B(S_xB_x + S_yB_y + S_zB_z) \tag{4.29}$$

where h is Planck's constant, D is the zero field splitting (ZFS), S_i and B_i denote the Cartesian components of the spin-1 operator and the magnetic field, respectively. The $\hat{z}$ axis is defined by the symmetries of the crystal and coincides with the c-axis.

In the absence of a magnetic field, the Hamiltonian is given by the ZFS term alone, whose eigenvectors are given by the eigenvectors of the operator S_z^2. Thus, the spin eigenvectors in the ground and excited states coincide, despite the ZFS constant D taking on different values. In this case, the overlap of the spin eigenfunctions in ground and excited states is given by

$$\langle g_j|e_i\rangle = \delta_{ij} \tag{4.30}$$

where δ_{ij} denotes the Kronecker delta. This means that only direct transitions ($|\phi_{e,i}\rangle \leftrightarrow |\phi_{g,i}\rangle$) are allowed. The same occurs if a magnetic field is applied along the $\hat{z}$ direction. In this case, the eigenvectors of both ground and excited states coincide with the eigenvectors of the operator S_z.

In contrast, if a magnetic field is applied at an angle with the c-axis, the sublevels of the ground(excited) state spin Hamiltonian are given by the eigenvectors of Eq. 4.29. In the basis $\{|+\rangle, |0\rangle, |-\rangle\}$ given by the eigenvectors of S_z (where $\hat{z}$ coincides with the crystal c-axis), this operator can be written in matrix form as

$$H_{g(e)} = \begin{bmatrix} hD_{g(e)} + g_{g(e)}\mu_B B\cos(\theta) & g_{g(e)}\mu_B B\sin(\theta) & 0 \\ g_{g(e)}\mu_B B\sin(\theta) & 0 & g_{g(e)}\mu_B B\sin(\theta) \\ 0 & g_{g(e)}\mu_B B\sin(\theta) & hD_{g(e)} - g_{g(e)}\mu_B B\cos(\theta) \end{bmatrix} \tag{4.31}$$

Here we assume that the magnetic field makes an angle θ with the crystal c-axis, and its component along the $\hat{y}$ axis is zero. This last assumption is allowed due to the symmetry of the defect. For a general θ different from 0 (i.e. for a magnetic field non-collinear with the c-axis), the eigenvectors of this operator depend on the value of the ZFS constant $D_{g(e)}$, such that the eigenvectors of ground and excited state Hamiltonians differ. In this case, the overlap between sublevels of ground and excited state $\langle g_j|e_i\rangle \neq \delta_{ij}$, and diagonal transitions ($|\phi_{g,j}\rangle \leftrightarrow |\phi_{e,i}\rangle$, for $i \neq j$) are allowed for arbitrary i and j.

We note finally the case of a magnetic field perpendicular to the crystal c-axis (parallel to the basal plane). In this case the angle is $\theta = \pi/2$ and the Hamiltonian given in Eq. 4.31 becomes

$$H_{g(e)} = \begin{bmatrix} hD_{g(e)} & g_{g(e)}\mu_B B & 0 \\ g_{g(e)}\mu_B B & 0 & g_{g(e)}\mu_B B \\ 0 & g_{g(e)}\mu_B B & hD_{g(e)} \end{bmatrix} \tag{4.32}$$

The lowest and upper eigenvectors of this operator depend on the value of $D_{g(e)}$ and are thus given by different vectors in ground and excited states. However, the middle eigenvector of this operator is given by $|g(e)_m\rangle = (|+\rangle - |-\rangle)/\sqrt{(}2)$ (which is an eigenvector of S_x and S_z^2), regardless of the value of $D_{g(e)}$ or $g_{g(e)}$.

Thus, this eigenvector is the same in the ground and excited states, i.e. $|g_m\rangle = |e_m\rangle$. Within ground and excited states, the eigenvectors of the Hamiltonian are orthogonal to each other (since $\langle g_m|g_{l,u}\rangle = 0$ and $\langle e_m|e_{l,u}\rangle = 0$). This means that $\langle e_m|g_{l,u}\rangle = \langle g_m|e_{l,u}\rangle = 0$. Thus, although diagonal transitions between the lower and upper sublevels of ground and excited states are allowed ($|\phi_{e,l}\rangle \leftrightarrow |\phi_{g,u}\rangle$ and $|\phi_{g,l}\rangle \leftrightarrow |\phi_{e,u}\rangle$), diagonal transitions into or out of $|g_m\rangle$ and $|e_m\rangle$ are forbidden.

We consider then a pump pulse used to excite the c-axis divacancies. Just before the pulse arrives in the sample, the population is entirely in the lowest level of the ground state. Since the overlap between the lowest level of the ground state and the middle level of the excited state is zero, the pump pulse is only able to excite population into the lowest and upper levels of the excited state. Thus, in this case the only relevant coherence in the system after the pump pulse arrives is the coherence between the lowest and upper levels of the excited state, such that only one characteristic frequency is present.

In contrast, if the magnetic field is applied at an angle $\theta \neq 0, \pi/2$, all optical transitions are allowed. In this case, population from the lowest level of the ground state can be excited into all three levels of the excited state. Thus, after the pump pulse arrives in the sample, all three sublevels of the excited state are populated, and the coherences in the system are characterized by three oscillating frequencies corresponding to the three energy differences between the sublevels of the excited state.